Development of a Simple Upper-Ocean and Sea-Ice Model

DAVID POLLARD, MARY L. BATTEEN[1] AND YOUNG-JUNE HAN

Climatic Research Institute, Oregon State University, Corvallis, OR 97331

(Manuscript received 9 July 1982, in final form 1 February 1983)

ABSTRACT

Results are described for three simple numerical models of the upper ocean and sea ice with prescribed atmospheric forcing. The ability of each model version to simulate the observed sea surface temperature (SST) is assessed as a basis of comparison for future coupled experiments with atmospheric GCM's.

The upper-ocean model versions range from a slab of fixed thickness to a variable-depth mixed layer above a variable exponential temperature gradient representing the seasonal thermocline. Sea-ice thickness is determined thermodynamically by local melting or accretion, and the effects of ice transport and leads are neglected. Each version is tested by integrating to equilibrium with horizontal advection neglected, using monthly climatological atmospheric data for a selected north–south section in the mid-Pacific Ocean, and the results for different model versions are compared with each other and with available observations.

It is found that the fixed-slab version gives realistic sea-ice thickness and extent, and temperatures within 1–2°C of observed SST's over much of the mid-Pacific. However, a variable-depth mixed layer is required to maintain this level of accuracy for summer SST's north of 40°N, and also to produce the correct phases of the annual cycles of temperature at all extratropical latitudes. Mixed-layer depths in the latter version are somewhat too shallow in winter, but the overall seasonal pattern agrees with that observed.

1. Introduction

The sea surface temperature (SST) and the distribution of sea ice are the two most important oceanic variables affecting the heat flux between the ocean and atmosphere. For some applications of atmospheric general circulation models (AGCM's) the fields of SST and sea ice can be specified, e.g., for the simulation of the present climate. For other applications such as the future climatic response to anthropogenic perturbations, these fields may change significantly from their present values and so should be calculated by an oceanic model, as for instance by a "swamp" ocean with zero heat capacity (Manabe and Wetherald, 1975), a model of the upper mixed layer alone (Manabe and Stouffer, 1980), or by an oceanic general circulation model (OGCM) (e.g., Bryan *et al.*, 1975). In principle, a coupled AGCM–OGCM is the best theoretical tool for such applications, but a step-by-step development using existing AGCM's coupled to various simple oceanic models may provide valuable preliminary results and may make more efficient use of computer resources.

In this report three versions of an upper-ocean model are described with increasingly complex treatments of the vertical structure of the seasonal thermocline. Each model is run with prescribed atmospheric forcing, with the main purpose being to assess the size and character of the errors in SST resulting directly from the simplifications in each model. These results can then form a basis of comparison for the minimum errors liable to occur when similar upper-ocean models are coupled to AGCM's in coupled equilibrium simulations of the present climate.

Advection is neglected in all model versions here. When such non-advective models are extended to a global domain and coupled to an AGCM, the largest SST errors caused by the neglect of advection occur near the oceanic western boundaries and in equatorial upwelling regions (Manabe and Stouffer, 1980). As shown by Gill and Niiler (1973) using scaling analysis, the neglect of advection in modelling the basic seasonal cycle of the upper ocean is a good approximation in mid-oceanic regions away from the equator. Mainly for this reason the results are limited here to a north–south transect in the mid-Pacific. All results will still contain some common errors due to the neglect of advection, but comparisons between the different model versions will then isolate those errors due to the simplifications in their *vertical* structure, i.e., the partitioning of the seasonal heat between the mixed layer and the thermocline.

The three upper-ocean models considered here are a fixed-slab mixed layer (version 1), a variable-depth mixed layer above a specified deep fluid (version 2), and a variable-depth mixed layer above a variable "thermocline" represented by exponential profiles (version 3). Each version has a variable sea-ice component. In Section 2 the basic model is formulated,

[1] Present affiliation: National Center for Atmospheric Research, Boulder, CO 80307.

and the earlier work relevant to each component of the model is described. In Sections 3 and 4 results are shown for a selected north–south section in the mid-Pacific Ocean, with surface fluxes calculated from climatological atmospheric data. Results for the three model versions are also compared with each other and with climatological observations. Some other features relevant to future coupled AGCM experiments are discussed in Section 5, and an extension of the model to include variable salinity under sea ice is described in an Appendix.

2. Previous work and present model formulation

a. The oceanic mixed layer

A comprehensive review of recent modelling of the upper ocean is provided in Kraus (1977). The reader is also referred to Heald and Kim (1979) who were concerned with the use of mixed-layer models over a global domain. The formulation below closely follows the development of several recent one-dimensional mixed-layer models that describe the effects of local surface fluxes and entrainment of (or detrainment to) the water below the mixed layer (e.g., Denman, 1973; Kim, 1976; Niiler and Kraus, 1977). Fig. 1 schematically shows the structure of the most complex version of our model (version 3), and the equations for this version are shown below; versions 1 and 2 are straightforward simplifications of version 3 (as described in Section 2c), and the various terms and equations to omit for the simpler versions should be apparent. The particular entrainment parameterization used here is described separately in Section 2b.

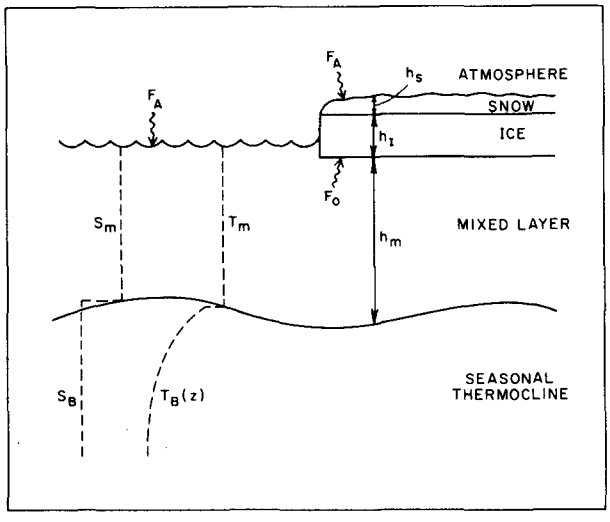

FIG. 1. Schematic structure of the model (version 3). Here h_m is mixed-layer depth, T_m mixed-layer temperature, s_m mixed-layer salinity (specified), h_I sea-ice thickness, h_S snow thickness, F_A atmospheric heat flux into the surface, F_0 oceanic heat flux into the ice (specified), T_B an exponential curve in depth (z) representing the temperature profile in the seasonal thermocline, and s_B salinity below the mixed layer (specified).

When the thermodynamic energy equation and the mass continuity equation are integrated vertically through the mixed layer (e.g., Niiler and Kraus, 1977) neglecting advection, they may be written

$$\frac{\partial T_m}{\partial t} = \frac{F_A - F_S e^{-\beta h_m}}{\rho_0 c h_m} - \frac{E^* \Delta T}{h_m}, \tag{1}$$

$$\frac{\partial h_m}{\partial t} = E. \tag{2}$$

Here t is time; T_m and h_m are the mixed-layer temperature and depth, respectively; E is the rate of entrainment or detrainment at the base of the mixed layer (see Section 2b), with $E^* = \max(0, E)$; $\Delta T = T_m - T_B(h_m)$ is the temperature jump across the base of the mixed layer, where $T_B(z)$ is the vertical temperature profile in the thermocline (see Section 2c); F_A is the net downward heat flux at the surface, computed from current atmospheric conditions using standard parameterizations (see Appendix A); F_S is the solar component of F_A and β is the solar extinction coefficient taken as 0.2 m^{-1}; and $\rho_0 = 1.025$ g cm^{-3} and $c = 0.977$ cal g^{-1} $(°C)^{-1}$ are the reference density and specific heat of sea water, respectively.

b. Entrainment parameterization

The parameterization of entrainment used here is a standard mixed-layer formulation (Niiler and Kraus, 1977), and differs from several previous parameterizations only in the coefficients used to represent the dissipation of turbulent kinetic energy. The physics described by these parameterizations is basically as follows. In order to maintain the (presumed) vertically uniform profiles of temperature and salinity in the mixed layer, vertical turbulent fluxes must exist to redistribute any non-uniform forcing such as surface heating or cooling, surface salinity flux, or entrainment of a different fluid type from below. When the resulting net buoyancy flux $(-\rho' w')$ is required to be downward, work must be done by the turbulence against gravity; conversely, if this flux is upward, potential energy is released and the turbulent kinetic energy would tend to increase. However, the variation of turbulent kinetic energy density is observed to be negligible compared to its sources and sinks, and so the vertically integrated turbulent kinetic energy equation can only be satisfied if the mixed layer deepens or shallows at the particular rate that results in a balance between these sources and sinks.

To implement this physical picture several fairly arbitrary parameterizations and parameter values for turbulent processes must be chosen. The net result is a diagnostic expression for the entrainment rate that can be tuned to yield reasonable seasonal cycles of mixed-layer depth. The present results address how the variation of mixed-layer depth affects the SST, but the validity and accuracy of the turbulent param-

eterizations themselves are beyond the scope of this paper.

The rate of entrainment ($E > 0$) or detrainment ($E < 0$) in the present model is given by

$$E = \frac{2ne^{-rh_m}\rho_0 v_*^3 - [\{F_A + F_S\pi(\beta h_m) - F_0\}\alpha c^{-1} + \{F_p - F_E\}\gamma s_m]gh_m}{\rho_0 C_m^{\,2} + \Delta\rho^* gh_m}. \quad (3)$$

Here $v^* = (|\tau|/\rho_0)^{1/2}$ is the friction velocity with τ the wind stress; $n = 3.0$ is an empirical coefficient; and $r^{-1} = 20$ m is the penetration depth against turbulent dissipation. This form for the dissipation of wind-driven turbulence is that used by Kim and Gates (1980). The function π is defined as

$$\pi(\beta h_m) = e^{-\beta h_m} - 2(1 - e^{-\beta h_m})/\beta h_m$$

and represents the influence of penetrating solar radiation. The effect of the strong absorption of sunlight within the first meter of water (Jerlov, 1976) is neglected in (3), but its inclusion would not significantly affect the results found below since generally $h_m \gg \beta^{-1}$ (= 5 m). In (3), F_E is the rate of evaporation from the ocean surface, F_p is the rate of fresh-water supply due to precipitation and runoff (see Appendix A), and F_0 is the heat flux into the bottom of sea ice (see Section 2d); s_m is the mixed-layer salinity; $\alpha = -\rho_0^{-1}(\partial\rho/\partial T)$, $\gamma = \rho_0^{-1}(\partial\rho/\partial s)$ and $\Delta\rho$ are computed from Bryan and Cox (1972).

The turbulent velocity C_m in (3) is taken as max $\times$ ($3v^*$, 3 cm s^{-1}) as in Kim (1976), and $\Delta\rho^* = \Delta\rho$ if $E > 0$ and $\Delta\rho^* = 0$ if $E < 0$, where $\Delta\rho = \rho_B(h_m) - \rho_m$ is the density jump across the base of the mixed layer. Usually $\Delta\rho gh_m \gg \rho_0 C_m^{\,2}$ during entrainment, so for a given magnitude of the numerator in (3), entrainment rates ($E > 0$) are limited mostly by $\Delta\rho gh_m$. During detrainment ($E < 0$) in most mixed-layer models, the mixed-layer depth is supposed to shallow instantaneously so that the numerator in (3) remains at zero. However, Eq. (3) is still used here with detrainment rates limited (somewhat unphysically but to a good approximation) only by $\rho_0 C_m^{\,2}$ in the denominator, as in Kim (1976).

A few processes considered in some other studies are neglected in (3), such as the transfer of kinetic energy from the mean to the turbulent flow and the effect of inertia-gravity waves (e.g., Niiler and Kraus, 1977). However, as discussed by these authors, much of the uncertainty in parameterizations such as (3) lies in the coefficients representing the dissipation of turbulent kinetic energy. As in several earlier studies, any dissipation of the buoyancy-driven turbulence associated with the bracketed terms in (3) is neglected here. In some seasonal models this neglect could lead to an ever-increasing potential energy and/or infinite mixed-layer depth (Stevenson, 1979), but this does not occur in the present model presumably since temperatures within the thermocline are redistributed during detrainment without conserving potential energy [see (5)–(7) below].

Many mixed-layer models equivalent to (1)–(2) and entrainment parameterizations similar to (3) have been tested satisfactorily against observations at single locations and/or for limited times of the year. For instance, Gill and Turner (1976) have modelled the complete annual cycle at a single point, and Alexander and Kim (1976) have obtained reasonable simulations of mixed-layer depth during summer for the entire North Pacific using climatological atmospheric forcing. Several coupled atmosphere–ocean models have included variable mixed-layer treatments (e.g., Pike, 1971; MacCracken and Luther, 1974; Bryan *et al.*, 1975; Lau, 1978; Thompson and Schneider, 1979; Hunt and Wells, 1979; Wells, 1979). Kim and Gates (1980) have imbedded a mixed layer similar to ours into an OGCM, with the temperature just below the mixed layer extrapolated from the deeper OGCM levels. However, with the possible exception of Lau (1978), none of these models have yet focused on producing realistic simulations of the seasonal variations of the mixed layer on a global scale.

c. *The seasonal thermocline and model versions*

Since any fluid in the upper region of the thermocline may be entrained into the mixed layer at some later time, a detailed record of temperature versus depth below the mixed layer should ideally be retained, as in Kim (1976) for instance. In reality when detrainment occurs, the profile below the shallowing mixed layer is a record of the mixed-layer temperature as it shallows through each level. To carry this profile explicitly in a model, a fine vertical grid is needed which requires a relatively large amount of storage when the model is used on a global domain. This approach has been used by Wells (1979) with 20 oceanic layers of 10 m thickness at each grid point below an AGCM. In an attempt to develop an alternative approach with minimal storage requirements, we have experimented with various simplified thermocline treatments in three model versions:

VERSION 1. In this version the mixed layer is a fixed slab of 60 m thickness with no fluxes through its base, so all effects of entrainment and of the deep ocean are ignored.

VERSION 2. In this version the mixed-layer depth can vary and entrainment is given by (3), but the temperature below the mixed layer (T_B) is a specified function of latitude and is independent of depth. Also the salinity field in the mixed layer (s_m) and the sa-

linity below it (s_B) are specified functions of latitude ϕ. Here we use

$$\left.\begin{aligned} T_B\,(°C) &= 20\cos^4\phi, \quad s_m\,(‰) = 35 - 3\sin^4\phi \\ s_B\,(‰) &= 35 \end{aligned}\right\}. \quad (4)$$

These functions are chosen to correspond roughly to observed annual mean conditions in the mid-Pacific and Arctic Oceans at ~200 m depth for T_B and s_B and at the surface for s_m (Semtner, 1976a; Levitus and Oort, 1977).

VERSION 3. Most observed profiles in the seasonal thermocline (e.g., Turner and Kraus, 1967, Fig. 2) can be described fairly well at any one time by a single exponential, but the best-fit exponential at each location may vary in time. In version 3 the salinity is specified as in version 2, but below the mixed layer the temperature profile is given by

$$T_B = T_D + Ae^{-B(z-h_m)}, \quad (5)$$

where z is depth below the surface (positive downwards).

Physical constraints on the thermocline profile are (i) at depth the temperature tends to a seasonally invariant value, (ii) during detrainment there is no discontinuity across the base of the mixed layer, and (iii) net heat is conserved in the column. To satisfy these constraints in (5), T_D (°C) = $20\cos^4\phi$ to represent a fixed temperature at ~200 m depth as in version 2. A and B are adjusted at each time step to satisfy the two constraints

$$\frac{\partial}{\partial t}\left[\int_{h_m(t)}^{\infty}(T_B(z) - T_D)dz\right] = -E(T_B(h_m) - T_D) + \frac{F_S e^{-\beta h_m}}{\rho_0 c}, \quad (6)$$

$$\left.\begin{aligned} T_B(h_m) &= T_m \quad \text{if} \quad E < 0 \\ \frac{\partial}{\partial t}[T_B(h_m)] &= E\frac{\partial T_B}{\partial z}(h_m) + \frac{\beta F_S e^{-\beta h_m}}{\rho_0 c} \\ &\qquad \text{if} \quad E \geqslant 0 \end{aligned}\right\}. \quad (7)$$

Eq. (6) follows from the conservation of heat below the mixed layer, and Eq. (7) satisfies considerations of continuity at the mixed-layer base. In effect A and B are two prognostic variables for the seasonal thermocline at each grid point. As mentioned in Section 2b, potential energy is not conserved by this parameterization; this would require an additional degree of freedom in the thermocline profile (e.g., Miropol'skiy, 1970).

Eq. (5) is limited to profiles that are monotonic in depth, and so in high-latitude regions where the seasonal range of T_m straddles T_D and mixed-layer buoyancy is maintained by salinity, Eqs. (6) and (7) often cannot both be satisfied. Also in equatorial regions with relatively weak seasonal cycles, the equilibrium value of the e-folding depth B^{-1} tends to be very large ($\gg$200 m). For these reasons we are led to impose the following algorithm in addition to (6) and (7):

> Whenever (6) and (7) cannot both be satisfied or would require $B^{-1} > 100$ m, B^{-1} is reset to 100 m and (7) is allowed to be violated. However, if the resulting value of $T_B(h_m)$ lies outside the temperature range of the previous profile, $T_B(h_m)$ is reset to the closest extreme value of the previous profile and (6) is also allowed to be violated. (8)

The use of the algorithm (8) is *ad hoc*, but is required for our simple thermocline model to be applied globally. Eq. (8) can result in a gain or loss of heat in the seasonal thermocline, which can be considered as roughly analogous to the influence of the deeper ocean (see Section 5c).

Convective overturning between the mixed layer and seasonal thermocline can occur in versions 2 and 3 if $\Delta\rho$ becomes negative, and can be calculated as an adjustment after each time step (e.g., Kim, 1976). However, for simplicity in interpreting the initial results of the model shown below, the prescribed values of s_m, s_B and T_D in (4) were chosen (somewhat arbitrarily) so that $\Delta\rho$ always remains positive by a slight margin and so that convective overturning is insignificant.

Fig. 2 shows an example of the seasonal cycle of temperature versus depth at a single point in the mid-Pacific produced by version 3 of the model after an equilibrium annual cycle has been attained. The algorithm (8) does not come into effect at this location. This cycle compares reasonably well with many of the general features in seasonal data (e.g., Fig. 2 of Turner and Kraus, 1967). However, these data show a slight warming throughout the seasonal thermocline above approximately 150 m during late summer and fall when the mixed layer is already deepening, perhaps due to downward diffusion across the bottom of the mixed layer. This process is neglected in our present formulation, but could easily be incorporated into (1) and (6) (cf., Posmentier, 1980).

Our most complex thermocline (version 3) can still only simulate the "climatological" seasonal thermocline. It does not have enough degrees of freedom to describe the multiple jumps that accumulate below the mixed layer due to synoptic forcing, especially in summer (Denman and Miyake, 1973, Fig. 6), nor can it describe the daily thermocline just below the mixed layer caused by the diurnal insolation cycle (Denman, 1973; Kim, 1976). For this reason daily-mean atmospheric forcing was used in evaluating the numerator of (3) for all results shown here. The inadequacy of the model for the diurnal cycle of mixed-layer depth should not be serious for most climatic applications of coupled models, since the diurnal

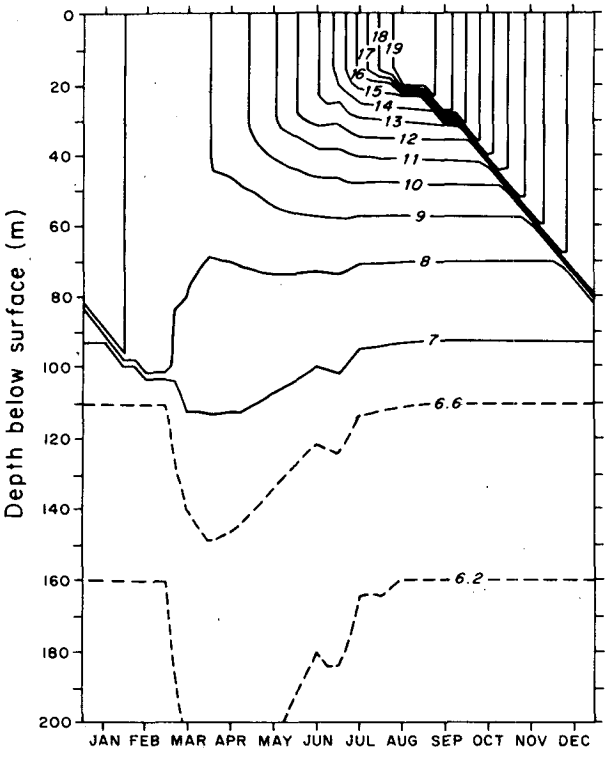

FIG. 2. Temperature (°C) as a function of depth and month at 42°N, 170°W, simulated by model version 3 (variable thermocline). (Discontinuities across the mixed-layer base that exist for part of the year appear smoothed due to the finite resolution of the plotting routine.)

variation of SST is generally very small compared to its synoptic, seasonal and probably its climatological variations.

d. Sea ice

The sea-ice model follows the recent development of a series of one-dimensional (vertical) models in which the ice thickness is determined by local melting or accretion of the top and/or bottom surfaces. Semtner (1976b) found that models with only very coarse vertical resolution of internal ice temperature profiles (or even with ice thermal capacity neglected altogether) yielded essentially the same results for ice thickness as those from Maykut and Untersteiner's (1971) model with much finer vertical resolution. Pease (1975) had previously used a similar model to Semtner's simplest version to simulate the seasonal ice variation along a north–south section in the Antarctic Ocean. Parkinson and Washington (1979) added horizontal ice transport and a parameterization for subgrid-scale "leads" (i.e., cracks exposing the ocean), and tested the resulting model for the Arctic and Antarctic using climatological atmospheric forcing. They obtained a realistic thickness and geographic distribution of sea ice, and also found that the neglect of horizontal ice transport had little effect on their results. [However, Gordon and Taylor (1975) have argued that ice transport due to wind stress is important around Antarctica, and Hibler (1979) has found significant effects of transport in the Arctic using a dynamically more sophisticated sea-ice model.] Simple ice-thickness models similar to that used here have also been used in OGCM's by Bryan *et al.* (1975) and Washington *et al.* (1980).

Our model is basically Semtner's simplest version (his "0-layer"), with ice transport, leads, internal ice temperature, penetrating radiation and brine pockets all neglected. The prognostic equation for ice thickness h_I can apply either to bare ice or to ice covered by a layer of snow of thickness, h_S, i.e.,

$$\frac{\partial h_I}{\partial t} = -m_I - s_I + \frac{1}{\rho_I L_f}\left[\frac{T_F - T_g}{(h_I k_I^{-1} + h_S k_S^{-1}} - F_0\right]. \quad (9)$$

Here m_I and s_I are the rates of ice melted and sublimated (respectively) by atmospheric fluxes at the top of bare ice, and the term in brackets represents melting or accretion at the bottom of the ice. T_g is the temperature at the top surface of the ice or snow, T_F is the temperature of the bottom surface of the ice (constrained to be at the freezing point of sea water, taken as −1.7°C), F_0 is the oceanic heat flux into the bottom of the ice (see below), $\rho_I = 0.9$ g cm^{-3} is the density of sea ice, L_f is the latent heat of fusion (79.8 cal g^{-1}), and k_I and k_S are the thermal conductivities of ice and snow, taken as 5.4×10^{-3} and 3.94×10^{-4} cal cm^{-1} s^{-1} (°C)$^{-1}$, respectively.

The mean values of m_I, s_I, T_g and h_S for each time step are usually calculated from current atmospheric conditions using a diagnostic surface energy-balance equation (e.g., Semtner, 1976b). Since the present model is intended to be coupled to the OSU AGCM, we have used the relevant surface energy equation and parameter values in Schlesinger and Gates [1979, Eq. (21)]. Although this is actually a prognostic equation for T_g with a 1 h time step, its use should not cause any significant difference from the diagnostic equations used in other sea-ice models. In general ice can form at any grid point after the mixed-layer temperature T_m has dropped to the freezing point T_F. Any subsequent net heat loss from the mixed layer is balanced by the freezing of ice with T_m set equal to T_F. However, the denominator $h_I k_I^{-1} + h_S k_S^{-1}$ in (9) can be arbitrarily small for small h_I; to avoid computational difficulties, we therefore use (9) only after the ice has reached a thickness of 5 cm. For $0 < h_I < 5$ cm, atmospheric fluxes are computed as if for the open ocean.

As discussed by Pease (1975) and Parkinson and Washington (1979), the turbulent heat flux F_0 from the ocean into the bottom of the ice has a significant effect on ice thickness and distribution. However, the value of this flux depends not only on the effective

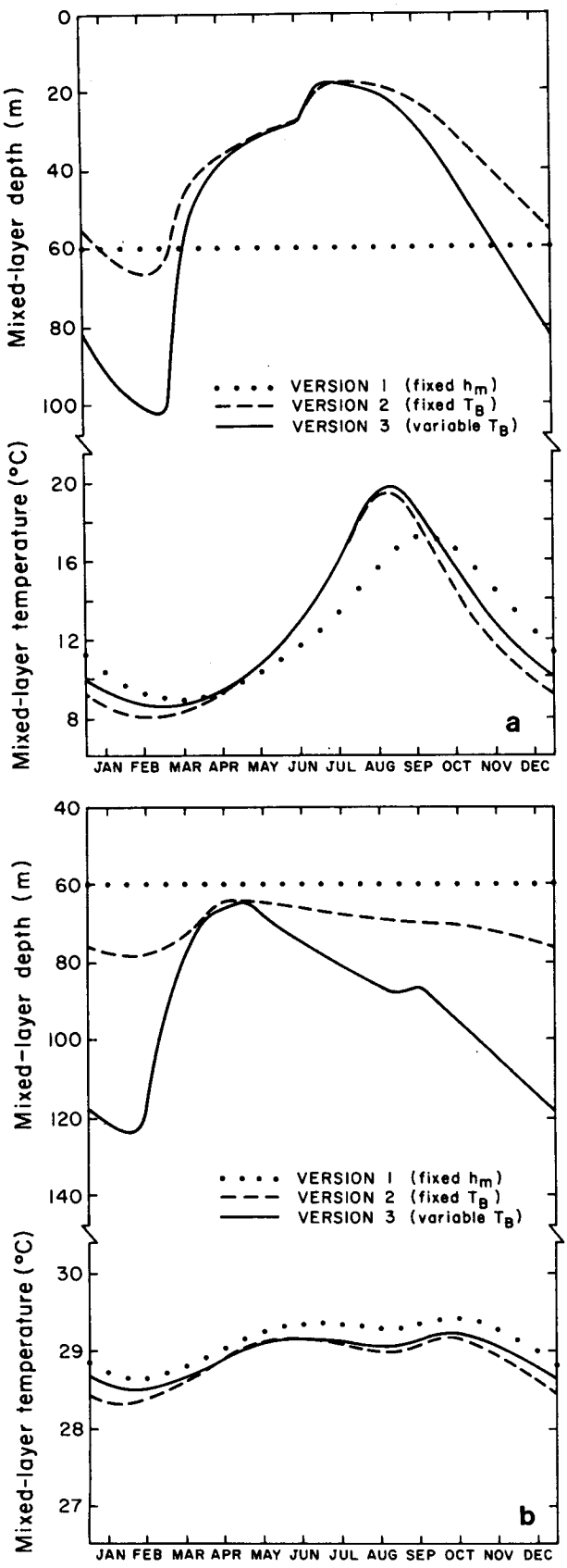

FIG. 3. Seasonal variation of mixed-layer temperature and depth at (a) 42°N, 170°W and (b) 2°N, 170°W for the three model versions.

heat transfer coefficient between the ice and the mixed layer, but also on the entrainment of warmer and more saline intermediate water below the mixed layer. This entrainment depends on the fraction of the wind stress that is transmitted through the ice and on the salinity jump across the bottom of the mixed layer, which in turn depends partly on runoff into the polar oceans. In Appendix B, a preliminary attempt is made to model all these processes with F_0 dependent on mixed-layer temperature. However, for the main part of this report, as in Parkinson and Washington (1979), we do not attempt to predict the mixed-layer temperature under sea ice and simply specify F_0 as 2 W m^{-2} in the Arctic and 15 W m^{-2} in the Antarctic, with the mixed-layer temperature set equal to freezing whenever sea ice is present. The mixed-layer depth can still vary under sea ice according to (3), with F_A, F_S and F_E all zero. Since ice dynamics are neglected, we cannot predict the stress between ocean and ice (c.f., Hibler, 1979). As a rough approximation we assume that 100% of the wind stress τ is transmitted unmodified through the ice, as if the ice had no strength.

3. Application of the model at selected locations (point results)

In Fig. 3 the seasonal variation of mixed-layer temperature and depth produced by the three model versions are compared for two points (2°N and 42°N, 170°W), in the mid-Pacific. These two locations are sufficient to illustrate the major differences due to the different model versions, while more extensive results are given in Section 4 where comparisons with observations are also made. In Fig. 3, as in all results in this study, the model has been run long enough to achieve an equilibrium seasonal cycle (after ~3 to 10 years depending on the latitude and model version), with no horizontal advection or diffusion, and with salinity specified (except in Appendix B). For simplicity one year is approximated as 360 model days with twelve 30-day months, and a 24 h time step is used. However, a shorter time step (or an implicit backward scheme) is required by (3) during periods of rapid detrainment.

At 42°N in Fig. 3a, the shallowing of the mixed layer in spring and early summer in versions 2 and 3 temporarily causes a lower mixed-layer thermal inertia and results in maximum temperatures ~2°C warmer than with the fixed slab of version 1. This is basically the same warming effect as that found by Wetherald and Manabe (1972) in their seasonal coupled model. In the fall and winter in Fig. 3a, the entrainment of cold thermocline water causes the

minimum temperatures to be ~1°C cooler in versions 2 and 3 than with the fixed slab. These effects combine to produce an approximate 30% increase in the seasonal amplitude and an advance of the phase of the seasonal temperature cycle, with extreme temperatures occurring about 1 month earlier in summer and about 2 weeks earlier in winter than in the case of the fixed-slab version (cf., Thompson, 1976, Fig. 5).

The mixed-layer depth in version 2 is less than in version 3, and has a smaller seasonal cycle. This is because version 2 generally has a larger temperature jump across the bottom of the mixed layer due to the fixed thermocline temperature T_B (°C) = 20 $\cos^4\phi$ (=6.1°C at 42°N), which reduces entrainment through the $\Delta\rho^*$ term in (3). Entrainment of this colder thermocline fluid in version 2 produces a "fictitious" cooling of the mixed layer, with temperatures in the winter ~0.8°C less than in version 3. This cooling can be reduced by increasing the value chosen for T_B, but cannot be avoided completely in version 2 since any choice of fixed T_B (even with depth-dependence) is limited from above by the necessity to avoid excessive convective overturning.

The curves for 2°N in Fig. 3b show much the same model-dependent trends as in Fig. 3a, but now with the smaller seasonal variations of the tropics. In version 3 the mixed-layer depth still has a substantial seasonal variation compared to that of temperature, and consequently the equilibrium e-folding depths of the thermocline profile reach our arbitrary upper limit of 100 m and the algorithm (8) comes into effect during about half of the year. As mentioned above, this implicitly causes a cooling ("from the deep ocean"), requiring a net annual positive heat flux from the atmosphere and a reduction of temperature of version 3 compared to version 1.

The results for version 3 in Fig. 3a generally agree with those for 35° latitude in Hunt and Wells (1979), who used a more detailed model of the seasonal thermocline. The main difference is that their mixed-layer depth plunges below 100 m for two months in winter, reaching a maximum depth of ~200 m. Similar maximum depths in our model can also be obtained by adjusting our choices for T_D, s_m and s_B, or by allowing salinity to vary as described below in Appendix B.

4. Application of the model at a selected longitude (section results)

For the main initial testing of the model, a particular north–south section was chosen in the mid-Pacific, running from 70°S to 90°N. The choice of the mid-Pacific avoids regions where advection and upwelling have obviously strong effects on the SST and the extent of sea ice, such as the Norwegian Sea. The longitude line 160°E was chosen in the Southern Hemisphere to avoid the influence of ice flow from the Ross ice shelf, and 170°W was chosen in the Northern Hemisphere to pass through the Bering Straits; the discontinuity at the equator has no significance for the present purposes and is ignored in the figures which follow.

Fig. 4 shows results using a 60 m thick fixed slab (version 1), along with the observed monthly mean climatological SST's and ice extents for the particular north–south section. A latitudinal resolution of 4° was used to generate these figures. In Fig. 4a the Southern Hemispheric mixed-layer temperatures are within 1°C of the observed SST, but northward of 40°N summer temperatures are some 2–5°C colder than observed, and maximum temperatures occur ~1 month too late. Sea-ice limits in Fig. 4b are close to those observed, and the ice thicknesses are similar to the results of Parkinson and Washington (1979). As these authors note, these ice thicknesses generally agree with available data, but the scarcity of observations and the large interannual variability of seasonal ice permit only a rough testing of the sea-ice models. The maximum Arctic ice thicknesses in Fig. 4b are displaced from the pole to 86°N mainly because of a corresponding shift in the distribution of summer air temperatures in the data set used, and a similar displacement is seen in the results of Parkinson and Washington (1979). The multi-year cycles of ice thickness discovered by Semtner (1976b, Fig. 8) occur at a few locations in our model with periods of 2–4 years, for instance at 74 and 78°N for the run in Fig. 4b; at these locations the ice thicknesses at the beginning of the year shown are different from those shown at the end of the year. These cycles depend on the insulating effect of seasonal snow, and can occur only in the transition zone between perennial ice and seasonal ice.

Fig. 5 shows results for version 2 (specified thermocline), and Fig. 6 for version 3 (variable thermocline). The model-dependent effects illustrated in Fig. 3 are seen throughout Figs. 4–6. The addition of a variable mixed-layer depth for Figs. 5 and 6 improves the predicted summer temperature in the Northern Hemisphere, especially north of 55°N as seen in the 5°C isotherm. However, the seasonal amplitudes of temperature around 40°S and 40°N in Figs. 5a and 6a are now slightly larger than observed, and a better fit was in fact obtained in Fig. 4a by the fixed-slab model. Perhaps a more significant improvement over the fixed-slab model is the correct prediction in Figs. 5a and 6a of the seasonal phases of the temperature cycles at all extratropical latitudes. The ice extents in Figs. 4–6 are insensitive to the mixed-layer version used (recalling that the vertical heat flux into the bottom of the ice is fixed), and the ice thicknesses for version 2 and 3 (not shown) are nearly the same as those shown in Fig. 4b.

Mixed-layer depths in Fig. 5b are much too shallow

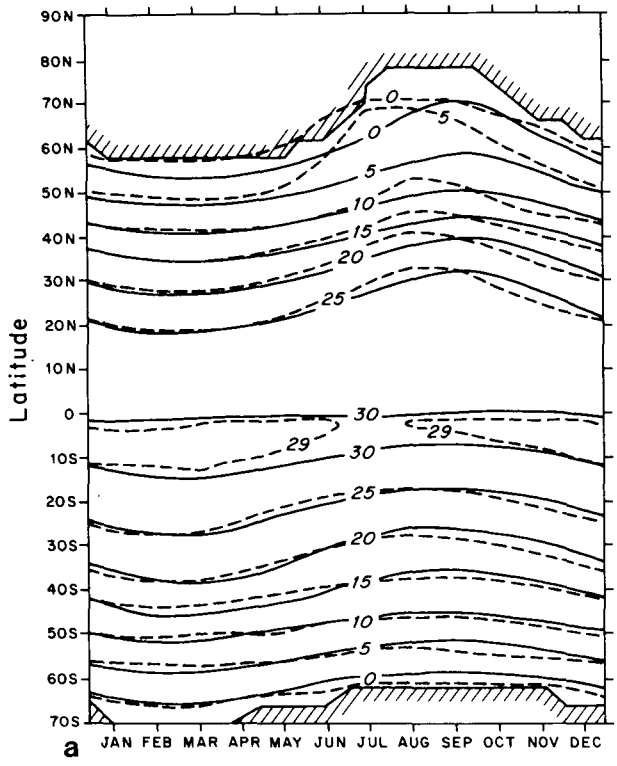

FIG. 4a. Solid lines: Mixed-layer temperature (°C) for model version 1 (fixed slab). The hatched line shows the most equatorward ice-covered points produced by the model on the 4° latitudinal grid. Dashed lines: Observed climatological SST (°C) for the particular north–south section, interpolated from NCC and NAVAIR data as described in Appendix A. The observed 0°C and 5°C isotherms have been modified slightly to agree with SST data in Alexander and Mobley (1974).

in winter and in the tropics compared to Bathen's (1972) Northern Hemispheric data, which are shown for comparison in Fig. 7. With the variable thermocline in Fig. 6b, these depths are much closer to those observed but are still too shallow, by ~30% equatorward of 40°N and by ~100% poleward of 40°N. As Bathen notes, the halocline was not considered in obtaining his data so his winter depths in high latitudes may be deeper than would be indicated from density computations. This could account for much of the discrepancy in Fig. 6b, where poleward of ~50° the winter depths are controlled by our prescribed salinity fields with a permanent stabilizing jump [$=5 \sin^4\phi$ (‰)] across the base of the mixed layer. In addition, we note that our conservative choices of salinity and deep temperature fields in (4) can easily be tuned (or the salinity made variable) so as to produce winter depths of up to ~200 m at most latitudes (not shown).

Apart from the region poleward of ~50°N, the general patterns in Figs. 5b and 6b do, however, agree encouragingly with Bathen's data in Fig. 7; shallowing in spring begins at ~40°N and then spreads north and south as far as ~15°N by mid-summer, after which a general deepening begins in October. As discussed by Bathen, the relatively deep year-round mixed layers in low latitudes occur simply because of the lack of any strong seasonal heating and associated periods of rapid detrainment.

5. Discussion

a. *Model sensitivity*

In the above we have concentrated on the sensitivities of the results to the different thermocline treatments in model versions 1, 2 and 3, and now we turn briefly to the sensitivities of other parameter variations. Mixed-layer temperatures are, of course, quite sensitive to the parameterizations used to obtain surface heat fluxes from current atmospheric conditions, but a comprehensive discussion of the accuracy of these parameterizations and of the atmospheric data used is beyond the scope of this report. For a given set of surface fluxes, the temperature is quite insensitive to reasonable changes in the oceanic parameters (such as $T_D = 10 \cos^4\phi$, $\beta^{-1} = 20$ m), and changes by $\leqslant \pm 2$°C which is comparable to the differences among the model versions in Fig. 3.

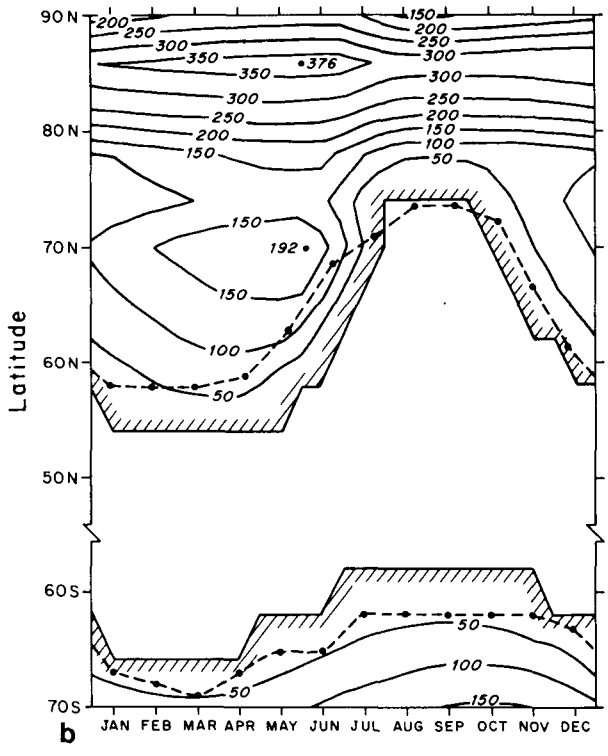

FIG. 4b. Ice thicknesses (cm) for model version 1 (fixed slab). The solid hatched line shows the most poleward ice-free grid points produced by the model on the 4° latitudinal grid, and the dashed line shows the observed monthly sea-ice limits (>0.5 fractional coverage) from Alexander and Mobley (1974).

The sensitivity of summer mixed-layer depths to changes in some of the atmospheric-forcing coefficients in the numerator of (3) is described by Alexander and Kim (1976, Figs. 6–8); for reasonable changes in these coefficients (e.g., β^{-1} = 20 m, n = 10) the depths vary by factors of ≤ 2. Mixed-layer depths in winter can be affected to a similar degree by these changes, and also by our choices of salinity and deep temperature fields s_m, s_B and T_D, which can be adjusted to produce winter depths from ~100 to 200 m at most locations in version 3.

Ice thickness and extent are generally insensitive to the different model versions, but as mentioned above this is probably imposed to some extent by fixing the value of the heat flux into the bottom of the ice. Perennial ice thicknesses in the central Arctic, currently around 300 cm, are sensitive to the value chosen for this flux, and also to factors that influence the amount of melting in the short polar summer, such as ice albedo, atmospheric heat transfer and snowfall. This sensitivity has been explored in detail by the earlier sea-ice studies mentioned in Section 2d; reasonable parameter variations can produce perennial ice thicknesses from 0 to ~7 m. Due to this large sensitivity, an accurate parameterization of the ocean-to-ice heat flux remains an important goal for future work.

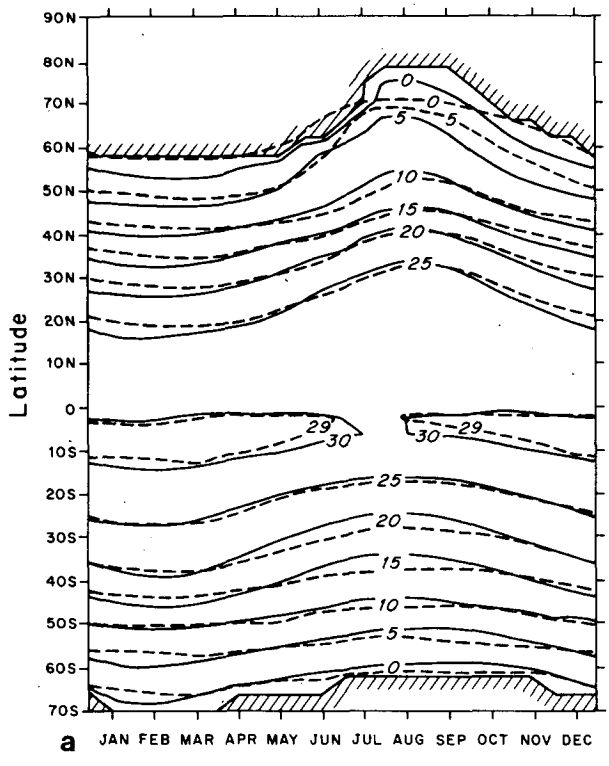

FIG. 5a. Solid lines: Mixed-layer temperature (°C) and sea-ice extent for model version 2 (specified thermocline). Dashed lines: Observed climatological SST (°C) as in Fig. 4a.

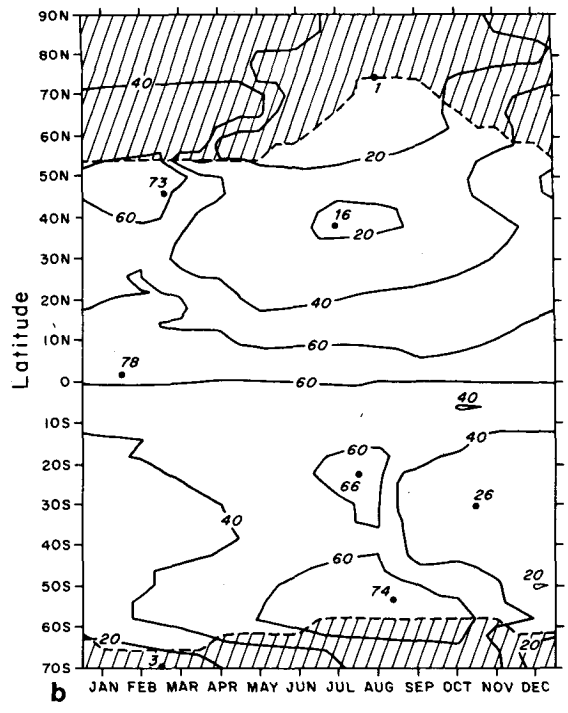

FIG. 5b. Mixed-layer depth (m) for model version 2 (specified thermocline). The regions poleward of the last ice-free grid points are shaded, since the model's prediction of mixed-layer depth under sea ice is relatively crude (see Section 2d).

As discussed in Section 2c, our thermocline treatments cannot describe the daily thermocline, and so daily-mean atmospheric forcing in calculating the numerator in (3) is used for all results shown here. If the diurnal cycle of insolation is retained, the mixed-layer depth in versions 2 and 3 varies by ~2–10 m every day, producing unrealistic mixing with the thermocline and unrealistic shallowing of the daily-mean depth. These effects combine to change temperatures by up to 2°C and mixed-layer depths by factors of ≥ 2. To avoid these effects when the model is coupled to an AGCM, running means over periods $\geq$ 24 h of atmospheric conditions or of surface fluxes in (3) will be used over the ocean.

The mixed-layer temperatures predicted by the fixed-slab model in Fig. 4a could have been made more realistic by allowing the (time-invariant) slab thicknesses to vary with latitude, as for instance in the zonal climate model of MacCracken and Luther (1974). However, it is felt that such a model would still be potentially less accurate than a (time) variable-depth, mixed-layer model such as version 3, as illustrated in Fig. 8 for the particular point 42°N, 170°W. Here the amplitudes of the seasonal temperature cycles produced by fixed slabs of 30 and 60 m bracket the observed amplitude, but the peak temperatures still occur either too late in summer or too early in winter. Although the amplitude produced by the vari-

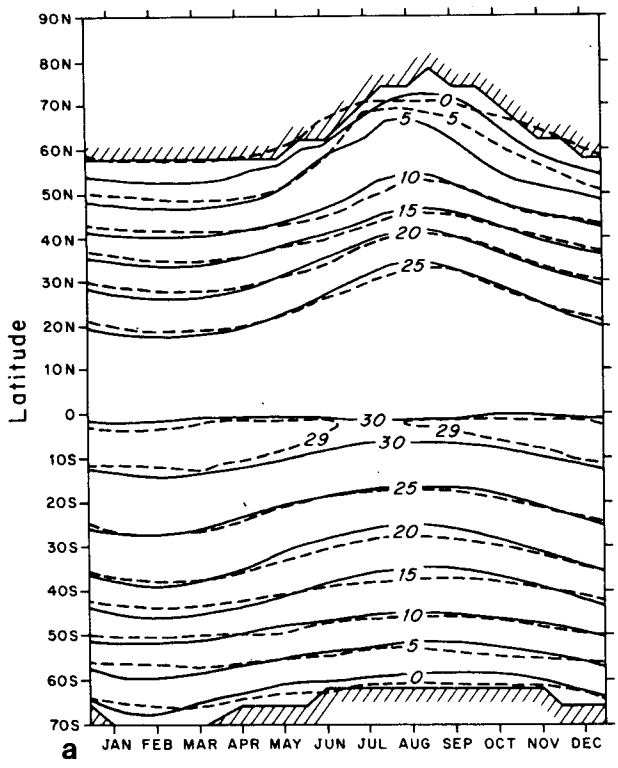

FIG. 6a. Solid lines: Mixed-layer temperature (°C) and sea-ice extent for model version 3 (variable thermocline). Dashed lines: Observed climatological SST (°C) as in Fig. 4a.

able-depth model is somewhat too large (which could be improved by further tuning), the hysteresis between the total heat content and the mixed-layer temperature inherent in the variable-depth model has resulted in summer and winter phases much closer to those observed.

b. *Spin-up times*

The response time of an AGCM to fixed changes in SST is roughly 30 days (Washington and Chervin, 1980). With the addition of the much greater thermal inertia of an upper ocean, the response time of a coupled model would be increased considerably. Minimum estimates of this response time are provided by the spin-up times in the present experiments to seasonal equilibrium with fixed atmospheric forcing.

For all results shown here, the model has been run from initial conditions obtained from the observed SST and ice distributions, until an equilibrium seasonal cycle has been attained (defined as at least within ~0.05°C in T_m and ~3 cm in h_l). The transfer coefficient for net heat exchange with the atmosphere is typically ~35 W m^{-2} (°C)$^{-1}$ (Haney, 1971), so with *prescribed* atmospheric conditions the e-folding time to equilibrium for the temperature of a 60 m thick water slab is ~90 days, resulting in spin-up times of ~3 years for version 1. The addition of a fixed thermocline in version 2 does not increase this spin-up time. With the variable thermocline in version 3, the temperature cycle does not change by more than ~0.2°C after ~3 years, but the mixed-layer depths and thermocline variables require some 7–10 years to reach equilibrium. In all models, the ice thicknesses reach equilibrium after about 3 years in regions with open ocean for part of the year. However, perennial ice thicknesses require ~10 years to adjust to within ~10 cm of equilibrium (unless initial thicknesses are chosen carefully).

These spin-up times apply to cases with prescribed salinity; as mentioned in Appendix B, cases with variable salinity require on the order of 20 years to reach equilibrium. Furthermore, these spin-up times are for prescribed atmospheric conditions. In a fully-coupled AGCM experiment, the atmosphere would vary in response to the changing oceanic conditions and the times required to reach equilibrium may be increased (cf., Manabe and Stouffer, 1980).

c. *Interaction with the deep ocean*

The results shown above for the various model versions indicate that a fixed-slab model can simulate the observed SST to within about 1°C over most mid-oceanic regions, but some regions such as the north-

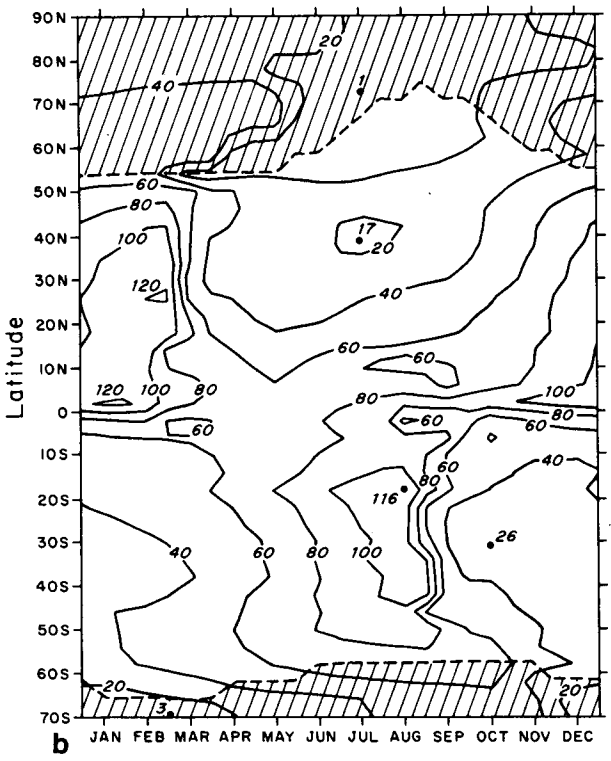

FIG. 6b. Mixed-layer depth (m) for model version 3 (variable thermocline). Sea-ice regions are shaded as in Fig. 5b.

ern mid-Pacific require the addition of at least a variable-depth mixed layer to maintain this level of accuracy. However, the use of prescribed atmospheric conditions in this report has disguised one important difference among the model versions, namely the amount of (implicit) net heat exchange with the deep ocean. Fig. 9 shows the net annual thermal and latent heat flux from the atmosphere into the upper surface of the model for the runs shown in Figs. 4–6. Since there is no horizontal advection here, any non-zero flux implies a local heat loss or gain in the thermocline that can be considered as an implicit heat exchange with the deep ocean. With the fixed slab of version 1, the heat flux in Fig. 9 is of course zero, except where sea ice occurs due to the prescribed flux F_0 in (9). With version 2 the heat fluxes are unrealistically large due to the fixed thermocline temperatures in (4). With version 3 the algorithm (8) results in downward net heat fluxes of ~ 12 W m^{-2} in low latitudes.

As mentioned in Section 2c, Eq. (8) used with version 3 is *ad hoc* and not a physical description of heat exchange with the deep ocean. The resulting heat fluxes in Fig. 9 are still unreasonably large (corresponding to a 1°C increase in the low-latitude deep ocean temperatures within ~50 years), and illustrate the need to improve the treatment of the main thermocline–deep ocean connection in version 3. The unrealistic net annual fluxes in Fig. 9 are not expected to have affected the SST results here by more than 0.5°C since the effective surface heat transfer coefficient is typically 35 W m^{-2} (°C)$^{-1}$ as noted above.

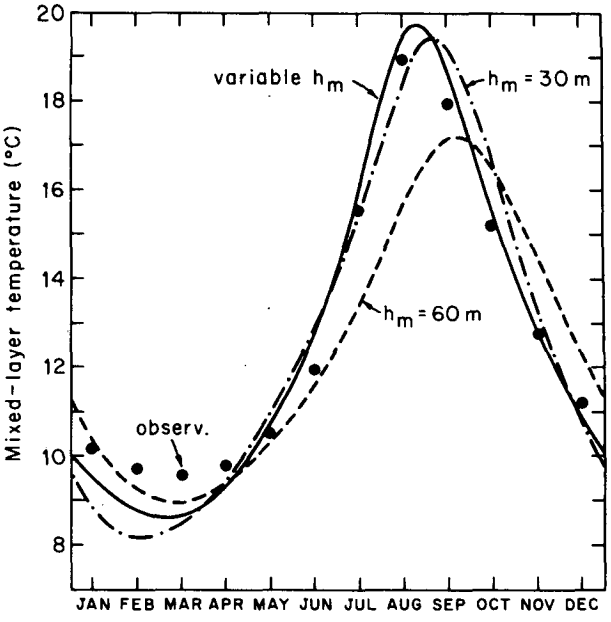

FIG. 8. Mixed-layer temperatures for 42°N, 170°W. Dashed line: fixed-slab model (version 1, h_m = 60 m); dashed-dotted line: fixed-slab model (version 1, h_m = 30 m); solid line: variable depth model (version 3); dots: observed monthly-mean SST (as in Fig. 4a).

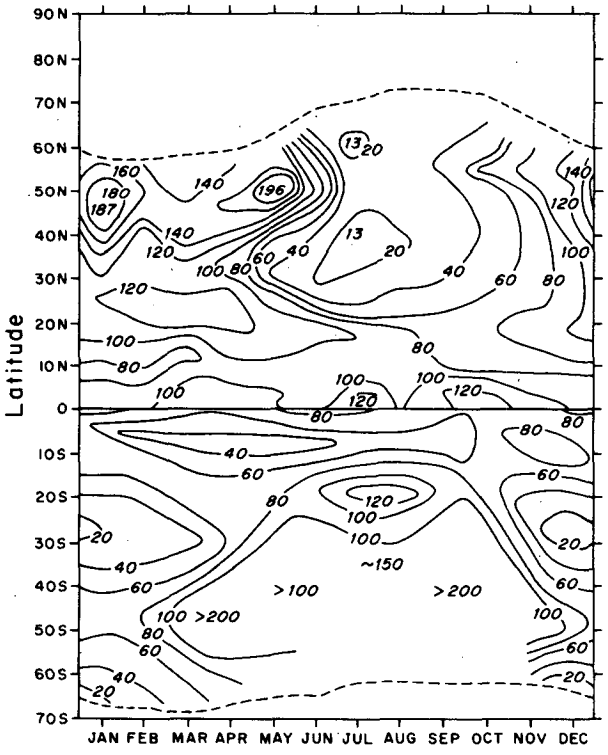

FIG. 7. Observed monthly-mean mixed-layer depth (m). Northern Hemispheric depths are for 170°W, redrawn from Bathen (1972). Since equivalent data for the South Pacific were unavailable, for completeness Southern Hemispheric depths are shown for 80°E (central Indian Ocean), redrawn from Wyrtki (1971). In both cases the mixed-layer depths were derived from temperature profiles alone. The dashed line shows the observed sea-ice limits as in Fig. 4b.

However, this shortcoming of version 3 would probably cause larger errors when the atmospheric forcing is not prescribed, and should certainly be corrected before coupling to an AGCM. The inclusion of advection in the model (e.g., Pike, 1971; De Szoeke, 1980) would also help to avoid large errors in equatorial upwelling regions and western boundary currents. With these caveats such a coupled model could be applied to problems with time scales of $\leqslant$100 years, i.e., as long as changes in the deep ocean are negligible.

Changes in the deep ocean strongly affect the transient response on time scales of several hundred years (Thompson and Schneider, 1979, Hoffert, *et al.*, 1980), and may also significantly affect the "quasi-equilibrium" climate on ice-age time scales ($\geqslant 10^4$ years). For these applications a full coupled AGCM–OCGM would probably be required, to capture both the thermal inertia of the deep ocean and changes in the thermohaline circulation. The upper-ocean results presented here may still be useful for OGCM applications, in assessing the importance of embedding a variable-depth mixed layer within the fixed

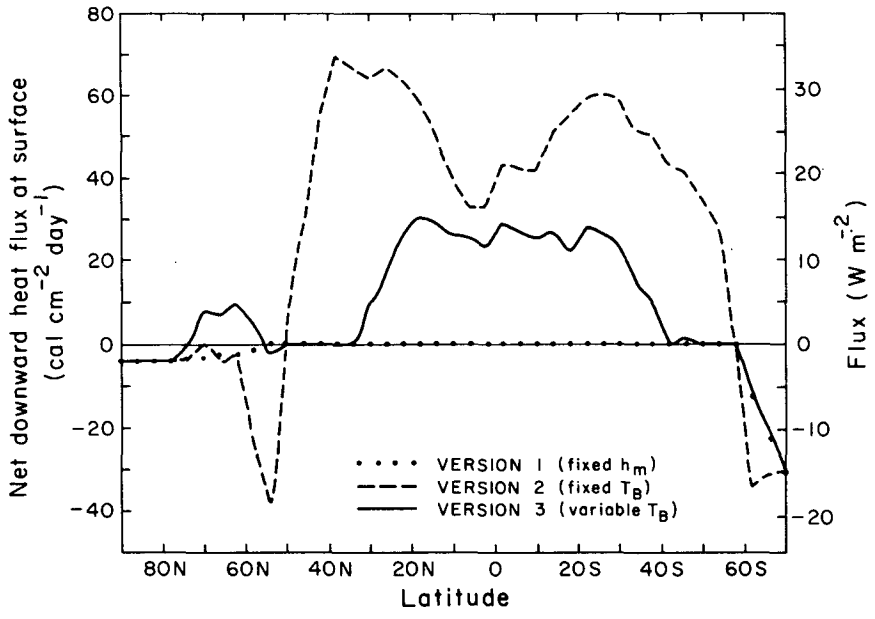

FIG. 9. The annual mean net thermal and latent heat flux at the surface (positive downward) predicted by several different model versions after an equilibrium annual seasonal cycle has been reached. This flux is defined for all surface types as $Q + I + H - L_v \times$ evaporation rate $- L_f \times$ snowfall rate, where L_v and L_f are 597.5 and 79.8 cal g^{-1}, respectively, and other symbols are defined in Appendix A.

vertical grid of an OGCM (Kim and Gates, 1980; Adamec *et al.*, 1981).

Acknowledgments. We would like to thank Jerry Olson for preparing much of the atmospheric data required for this work from the data sets described in Appendix A. Particularly helpful comments from an anonymous reviewer improved the manuscript and are much appreciated. We also thank Naomi Zielinski for typing the manuscript and Linda Haygarth for drafting the figures. This material is based on work supported by the following grants: Department of Energy/University of California Lawrence Livermore Laboratory Sub-Contract 8920109, National Science Foundation Grant ATM 80-01702, and NASA Grant NSG 5353.

APPENDIX A

Atmospheric Flux Parameterizations and Data Sets

1. Flux parameterizations

Fluxes into the surface of our model are given as diagnostic functions of the local atmospheric conditions and ground type. Most of the formulas and parameters below follow those in either Parkinson and Washington (1979) or Schlesinger and Gates (1979). The terms "surface air" or "surface wind" refer to atmospheric conditions at ~10 m elevation, and "ground" refers to one of the three surface types in this model: open ocean, bare ice or snow-covered ice.

The turbulent fluxes of sensible heat (H) and latent heat (E) into the ground are given by the bulk aerodynamic formulas

$$H = \rho_a c_a C_D v_a (T_a - T_g),$$

$$E = \rho_a L_v C_D v_a (q_a - q_g).$$

Here $\rho_a = [1/2.87T_a\,(°K)]$ g cm^{-3} and $c_a = 0.24$ cal g^{-1} (°C)$^{-1}$ are the surface air density and specific heat, respectively; T_a is surface air temperature, T_g is ground temperature (equal to the mixed-layer temperature for open ocean); q_a is the surface air specific humidity and q_g is the saturation specific humidity at the ground [with q_a obtained from the dew-point temperature T_d and q_g obtained from T_g using the same formulas as in Parkinson and Washington (1979)]; L_v is the latent heat either of vaporization (597.5 cal g^{-1}) for open ocean or of sublimation (677.3 cal g^{-1}) for ice or snow, and v_a is the surface wind speed. For ice or snow the transfer coefficient $C_D = 1.75 \times 10^{-3}$; for open ocean C_D is linearly interpolated from Table 4 in Bunker (1976), and depends on v_a and $T_a - T_g$; generally, its value over the ocean falls between 1.1×10^{-3} and 1.7×10^{-3}.

The downward net flux of infrared radiation at the surface (I) is calculated as in Parkinson and Washington (1979):

$$I = \epsilon_g I_0 (1 + 0.275 f_c) - \epsilon_g \sigma T_g^4.$$

Here I_0 represents the downward flux under cloudless skies, given as a function only of T_a [Parkinson and Washington, 1979, Eq. (5); Idso and Jackson, 1969]; ϵ_g is the ground's longwave emissivity, taken as 0.99 for a frozen snow surface and 0.97 otherwise; $\sigma = 1.355 \times 10^{-12}$ cal cm^{-2} s^{-1} (°K)$^{-4}$ is the Stefan-

Boltzmann constant; and f_c the fractional cloud cover.

The solar radiation absorbed at the surface (Q) is given by

$$Q = (1 - \alpha_g)Q_0(1 - 0.7f_c)/(1 - 0.7f_c\alpha_g),$$

where Q_0 is the solar radiation incident on the surface under cloudless skies (Parkinson and Washington, 1979, Eqs. (1)–(3); Zillman, 1972). The factors involving f_c are from Eq. (7) in Schneider and Dickinson (1976) and represent multiple reflections between the ground and "patchy" clouds with a cloud albedo of 0.7. The ground albedo α_g is taken as 0.1 for open ocean, 0.45 for bare ice and melting snow, and 0.8 for frozen snow. [We used the unusually low albedo of 0.45 for melting snow as a crude way of avoiding a sporadic problem encountered in earlier model runs involving unrealistic massive buildups of perennial snow in the central Arctic; in reality, snow-cover in the mid-Arctic melts away by late June (Hanson, 1965).]

The net downward heat flux at the surface, i.e., F_A in Eq. (1), is then given by $Q + I + H + E$, and the solar component F_S is Q. F_A is not the same as the flux shown in Fig. 9, since the latter is derived from a combined thermal and latent heat equation for the entire ice and water column, and includes the latent heats associated with all mass fluxes of water (evaporation and snowfall) choosing liquid as a base.

2. Data sets

In order to use the flux parameterizations in the present model tests, we required observed seasonal data for T_a, T_d, v_a and f_c along the particular north–south section in the mid-Pacific ocean from 70°S to 90°N. In addition, the magnitude of the surface wind stress τ was required in Eq. (3), the snowfall rate in the polar regions was needed for the calculation of h_s in (9), and the rate of fresh-water supply F_p due to precipitation and runoff was needed for (3).

Most of the data for T_a, T_d, v_a and τ were obtained from a monthly-mean climatological data set supplied by the National Climatic Center; this data set is designated TDF-11 and is described further in Bunker (1976). Since this set contained many points with missing temperature data in the polar regions (along our north–south section) we used NAVAIR data instead for T_a and T_d poleward of 50° latitude in both hemispheres (Taljaard *et al.*, 1969; Crutcher and Meserve, 1970). The patching of these two temperature data sets at 50° latitude was surprisingly smooth. Other missing data in the NCC data set were generated by linearly interpolating in latitude between surrounding NCC data points, with the values for our model grid obtained by subsequent linear interpolation. The monthly data at each latitude were taken to be valid for day 15 of each month, and the values for intervening times were obtained by linear interpolation.

The monthly fractional cloud cover f_c was determined from the processed satellite imagery in Miller and Feddes (1971). For high-latitude regions in each winter hemisphere not covered by this data, we used the somewhat simplified cloud cover used by Parkinson and Washington (1979). We also used Parkinson and Washington's prescribed snowfall rates for the Arctic and Antarctic. For the rate of fresh-water supply F_p we used constant values given by

$$F_p = \max(0.6 \sin^4\phi, 0.2) \text{ g cm}^{-2} \text{ day}^{-1},$$

where ϕ is latitude. This function crudely represents the observed annual mean precipitation rates in the north Pacific Ocean (Reed and Elliott, 1979) plus the annual runoff from rivers flowing into the Arctic Ocean (Semtner, 1976a).

APPENDIX B

Variable Salinity and Sea-Ice Heat Flux

Salinity was prescribed for all cases above mainly because the climatological mixed-layer buoyancy is controlled more by temperature than by salinity, except at high latitudes. Version 3 of the model can be extended to predict salinity, and preliminary results are presented here for a single point in the Arctic Ocean at 86°N, 170°W.

The spin-up times required to reach equilibrium for salinity in the polar regions are found to be typically ~20 years (on the order of the mixed-layer thickness divided by the fresh-water input rate), and is much longer than the spin-up times for other model variables (see Section 5b). Nevertheless it is important to predict salinity especially in the polar oceans, since it affects the distribution of sea ice through its influence on the heat flux (F_0) into the bottom of the ice, as discussed in Section 2d. Due to the many free parameters and simplifications in the model, especially the neglect of leads, horizontal advection and the use of single exponential profiles for the thermocline, the results presented below are regarded only as a preliminary demonstration that an equilibrium seasonal cycle and reasonable ice thicknesses can be obtained with variable salinity. Foster (1975) has performed a similar exercise using a vertically diffusing-convective ocean but with no explicit sea-ice component.

The equation for mixed-layer salinity (s_m), neglecting advection, is (e.g., Niiler and Kraus, 1977)

$$\frac{\partial s_m}{\partial t} = \frac{-E^*\Delta s}{h_m} + \frac{s_m}{\rho_0 h_m}(F_E - F_p), \qquad \text{(B1)}$$

where $\Delta s = s_m - s_B$ is the salinity jump across the bottom of the mixed layer, and other symbols are defined as in Sections 2a and 2b. Salinity in the seasonal thermocline is predicted using the exponential profiles and equations corresponding exactly to those for temperature in version 3 [Eqs. (5)–(8)].

As in Pease (1975) and some other models, the turbulent heat flux from the mixed layer into the bottom of the ice (F_0) occurring in (9) and (3) is now given by

$$F_0 = k(T_m - T_F), \qquad \text{(B2)}$$

with $k = 200$ W m^{-2} (°C)$^{-1}$; in this case F_0 is also included in (1) to cool the mixed layer. The net annual amount of this flux under perennial ice is ultimately limited in the model by the amount of heat transferred from the deep water (at temperature $T_D \approx 0$°C) to the thermocline according to the algorithm (8), and then from the thermocline to the mixed layer by entrainment. The "standard" model version 3 with variable salinity produced ice thicknesses of ~5 m for 86°N, so in order to produce realistic thicknesses we "tuned" the amount of heat flux from (B2) by increasing r^{-1} to 40 m in (3) and by using 50 m instead of 100 m as the upper limit for B^{-1} in (8). [The ice thicknesses were quite insensitive to the value of k in (B1).]

Fig. 10 shows the equilibrated seasonal cycle for year 20 of the run for 86°N. At this location the prescribed fresh-water supply F_p is 72 g cm^{-2} year^{-1}, mostly due to runoff (see Appendix A). This produces realistic salinities of ~30‰ in the mixed layer and is balanced by a net annual input of salt from the deep ocean via the algorithm (8). Any snow/ice melt or ice accretion computed by the model provides an additional seasonally-varying contribution to F_p that is included in (3) and (B1).

As shown in Fig. 10, warmer thermocline water is entrained into the mixed layer from August to the following June, thus providing heat to maintain significant amounts of the flux F_0. F_0 is largest during the initial period of rapid entrainment in September, and prevents any basal ice accretion until October. In early July rapid melting of snow and ice from the upper surface produces a large buoyancy flux and the mixed layer shallows rapidly to ~6 m depth, during which the algorithm (8) comes into effect and supplies some heat and salt to the thermocline for the next year's cycle. The annual mean of the heat flux F_0 turns out to be 2.2 W m^{-2}, which is close to the value 2 W m^{-2} prescribed for the standard model and thus ensures that the mean ice thickness in Fig. 10 is close to that in Fig. 4b.

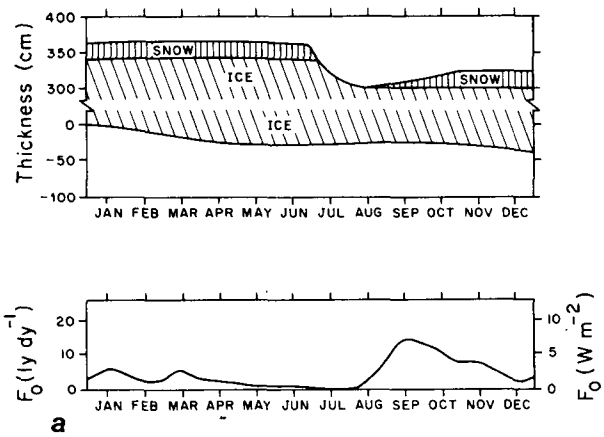

FIG. 10a. Seasonal cycle of ice thickness and oceanic heat flux at 86°N, 170°W, simulated by model version 3 (variable thermocline) but with variable salinity. The upper panel shows thickness variations for snow and ice, and the lower panel shows the turbulent heat flux from the mixed layer to the ice (F_0).

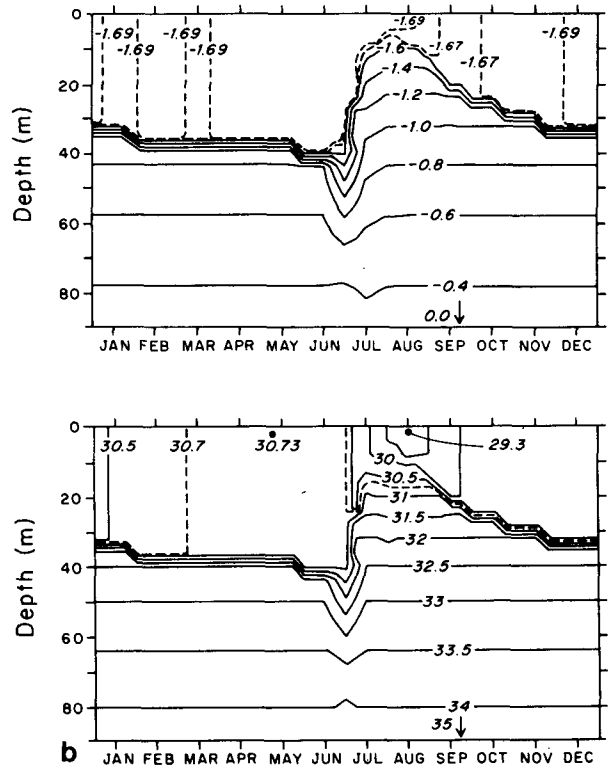

FIG. 10b. As in Fig. 10a except for the water temperature (°C, upper panel) and salinity (‰, lower panel) versus depth. (Discontinuities across the base of the mixed layer that exist for part of the year appear smoothed due to the finite resolution of the plotting routine.)

REFERENCES

Adamec, D., R. L. Elsberry, R. W. Garwood, Jr. and R. L. Haney, 1981: An embedded mixed layer-ocean circulation model. *Dyn. Atmos. Oceans*, **6**, 69–96.

Alexander, R. C., and J.-W. Kim, 1976: Diagnostic model study of mixed-layer depths in the summer North Pacific. *J. Phys. Oceanogr.*, **6**, 293–298.

——, and R. L. Mobley, 1974: Monthly average sea-surface temperatures and ice-pack limits on a 1° global grid. R-1310-ARPA, The Rand Corporation, Santa Monica, CA, 30 pp.

Bathen, K. H., 1972: On the seasonal changes in the depth of the mixed layer in the North Pacific Ocean. *J. Geophys. Res.*, **77**, 7138–7150.

Bryan, K., and M. D. Cox, 1972: An approximate equation of state for numerical models of the ocean circulation. *J. Phys. Oceanogr.*, **2**, 510–514.

——, S. Manabe and R. C. Pacanowski, 1975: A global ocean-atmosphere climate model. Part II: The oceanic circulation. *J. Phys. Oceanogr.*, **5**, 30–46.

Bunker, A. F., 1976: Computations of surface energy flux and annual air-sea interaction cycles of the North Atlantic Ocean. *Mon. Wea. Rev.*, **104,** 1122–1140.

Crutcher, H. L., and J. M. Meserve, 1970: *Selected Level Heights, Temperatures and Dew Points for the Northern Hemisphere.* NAVAIR Rep. 50-1C-52, U.S. Naval Weather Service Command, Washington, DC.

Denman, K. L., 1973: A time-dependent model of the upper ocean. *J. Phys. Oceanogr.*, **3,** 173–184.

——, and M. Miyake, 1973: Upper layer modification of ocean station PAPA: Observations and simulation. *J. Phys. Oceanogr.*, **3,** 185–196.

De Szoeke, R. A., 1980: On the effects of horizontal variability of wind stress on the dynamics of the ocean mixed layer. *J. Phys. Oceanogr.*, **10,** 1439–1454.

Foster, T. D., 1975: Heat exchange in the upper Arctic Ocean. *AIDJEX Bull.*, No. 28, 151–166 (unpublished manuscript).

Gill, A. E., and P. P. Niiler, 1973: The theory of the seasonal variability in the ocean. *Deep-Sea Res.*, **20,** 141–177.

——, and J. S. Turner, 1976: A comparison of seasonal thermocline models with observation. *Deep-Sea Res.*, **23,** 391–401.

Gordon, A. L., and H. W. Taylor, 1975: Seasonal change of Antarctic ice cover. *Science,* **187,** 346–347.

Haney, R. L., 1971: Surface thermal boundary condition for ocean circulation models. *J. Phys. Oceanogr.*, **1,** 241–248.

Hanson, A. M., 1965: Studies of the mass budget of Arctic pack-ice floes. *J. Glaciol.*, **5,** 701–709.

Heald, R. C., and J.-W. Kim, 1979: Parameterization of the ocean mixed layer for use in general circulation models. Rep. No. 10, Climatic Research Institute, Oregon State University, 48 pp.

Hibler, W. D., III, 1979: A dynamic thermodynamic sea ice model. *J. Phys. Oceanogr.*, **9,** 815–846.

Hoffert, M. I., A. J. Callegari and C.-T. Hsieh, 1980: The role of deep sea heat storage in the secular response to climatic forcing. *J. Geophys. Res.*, **85,** 6667–6679.

Hunt, B. G., and N. C. Wells, 1979: An assessment of the possible future climatic impact of carbon dioxide increases based on a coupled one-dimensional atmospheric-oceanic model. *J. Geophys. Res.*, **84,** 787–791.

Idso, S. B., and R. D. Jackson, 1969: Thermal radiation from the atmosphere. *J. Geophys. Res.*, **74,** 5397–5403.

Jerlov, N. G., 1976: *Marine Optics,* Elsevier, 231 pp.

Kim, J.-W., 1976: A generalized bulk model of the oceanic mixed layer. *J. Phys. Oceanogr.*, **6,** 686–695.

——, and W. L. Gates, 1980: Simulation of the seasonal fluctuation of the upper ocean by a global circulation model with an imbedded mixed layer. Rep. No. 11, Climatic Research Institute, Oregon State University, 60 pp.

Kraus, E. B., Ed., 1977: *Modelling and Prediction of the Upper Layers of the Ocean.* Pergamon Press, 325 pp.

Lau, K. M. W., 1978: Experiment with a simple ocean-atmosphere climate model: The role of the ocean in the global climate. *J. Atmos. Sci.*, **35,** 1144–1163.

Levitus, S., and A. H. Oort, 1977: Global analysis of oceanographic data. *Bull. Amer. Meteor. Soc.*, **58,** 1270–1284.

MacCracken, M. C., and F. M. Luther, 1974: Climate studies using a zonal atmospheric model. *Proc. Int. Conf. on Structure, Composition and General Circulation of the Upper and Lower Atmospheres and Possible Anthropogenic Perturbations,* Melbourne, Vol. II, 1107–1128. Edited by W. L. Godson, University of Melbourne, Australia.

Manabe, S., and R. T. Wetherald, 1975: The effects of doubling the CO_2 concentration on the climate of a general circulation model. *J. Atmos. Sci.*, **32,** 3–15.

——, and R. J. Stouffer, 1980: Sensitivity of a global climate model to an increase of CO_2 concentration in the atmosphere. *J. Geophys. Res.*, **85,** 5529–5554.

Maykut, G. A., and N. Untersteiner, 1971: Some results from a time-dependent thermodynamic model of sea ice. *J. Geophys. Res.*, **76,** 1550–1575.

Miller, D. B., and R. G. Feddes, 1971: *Global Atlas of Relative Cloud Cover, 1967–1970.* NOAA Nat. Environ. Sat. Serv. and USAF Environ. Tech. Appl. Center, Washington, D.C., 237 pp.

Miropol'skiy, Yu. Z., 1970: Nonstationary model of the wind-convection mixing layer in the ocean. *Izv. Atmos. Oceanic Phys.*, **6,** 1284–1294.

Niiler, P. P., and E. B. Kraus, 1977: One-dimensional models of the upper ocean. *Modelling and Prediction of the Upper Layers of the Ocean,* E. B. Kraus, Ed., Pergamon Press, 143–172.

Parkinson, C. L., and W. M. Washington, 1979: A large-scale numerical model of sea ice. *J. Geophys. Res.*, **84,** 311–337.

Pease, C. H., 1975: A model for the seasonal ablation and accretion of Antarctic sea ice. *AIDJEX Bull.*, No. 29, 151–172 (unpublished manuscript).

Pike, A. C., 1971: Intertropical convergence zone studied with an interacting atmosphere and ocean model. *Mon. Wea. Rev.*, **99,** 469–477.

Posmentier, E. S., 1980: A numerical study of the effects of heat diffusion through the base of the mixed layer. *J. Geophys. Res.*, **85,** 4883–4887.

Reed, R. K., and W. P. Elliott, 1979: New precipitation maps for the North Atlantic and North Pacific Oceans. *J. Geophys. Res.*, **84,** 7839–7846.

Schlesinger, M. E., and W. L. Gates, 1979: Numerical simulation of the January and July global climate with the OSU two-level atmospheric general circulation model. Rep. No. 9, Climatic Research Institute, Oregon State University, 102 pp.

Schneider, S. H., and R. E. Dickinson, 1976: Parameterization of fractional cloud amounts in climatic models: The importance of modeling multiple reflections. *J. Appl. Meteor.*, **15,** 1050–1056.

Semtner, A. J., Jr., 1976a: Numerical simulation of the Arctic Ocean circulation. *J. Phys. Oceanogr.*, **6,** 409–425.

——, 1976b: A model for the thermodynamic growth of sea ice in numerical investigations of climate. *J. Phys. Oceanogr.*, **6,** 379–389.

Stevenson, J. W., 1979: On the effect of dissipation on seasonal thermocline models. *J. Phys. Oceanogr.*, **9,** 57–64.

Taljaard, J. J., H. van Loon, H. L. Crutcher and R. L. Jenne, 1969: *Climate of the Upper Air: Southern Hemisphere,* Vol. 1, *Temperatures, Dew Points and Heights at Selected Pressure Levels.* NAVAIR Rep. 50-1C-55, U.S. Naval Weather Service Command, Washington, DC.

Thompson, R. O. R. Y., 1976: Climatological numerical models of the surface mixed layer of the ocean. *J. Phys. Oceanogr.*, **6,** 496–503.

Thompson, S. L., and S. H. Schneider, 1979: A seasonal zonal energy balance climate model with an interactive lower layer. *J. Geophys. Res.*, **84,** 2401–2414.

Turner, J. S., and E. B. Kraus, 1967: A one-dimensional model of the seasonal thermocline. 1. A laboratory experiment and its interpretation. *Tellus,* **19,** 88–97.

Washington, W. M., and R. M. Chervin, 1980: Response time of an atmospheric general circulation model to changes in ocean surface temperature: Implications for interactive large-scale atmosphere and ocean models. *Tellus,* **32,** 119–123.

——, A. J. Semtner, Jr., G. A. Meehl, D. J. Knight and T. A. Mayer, 1980: A general circulation experiment with a coupled atmosphere, ocean and sea ice model. *J. Phys. Oceanogr.*, **10,** 1887–1908.

Wells, N. C., 1979: A coupled ocean-atmosphere experiment: the ocean response. *Quart. J. Roy. Meteor. Soc.*, **105,** 355–370.

Wetherald, R. T., and S. Manabe, 1972: Response of the joint ocean-atmosphere model to the seasonal variation of the solar radiation. *Mon. Wea. Rev.*, **100,** 42–59.

Wyrtki, K., 1971: *Oceanographic Atlas of the International Indian Ocean Expedition.* National Science Foundation, Washington, DC, 531 pp.

Zillman, J. W., 1972: A study of some aspects of the radiation and heat budgets of the Southern Hemisphere oceans. *Meteor. Stud.*, No. 26, Bur. Meteor. Dept. of the Interior, Canberra, Australia, 562 pp.